OMTO, Volume *16*

Supplemental Information

Inhibition of USP14 Deubiquitinating Activity as a Potential Therapy for Tumors with *p53* Deficiency

Yu-Shui Ma, Xiao-Feng Wang, Yun-Jie Zhang, Pei Luo, Hui-Deng Long, Liu Li, Hui-Qiong Yang, Ru-Ting Xie, Cheng-You Jia, Gai-Xia Lu, Zheng-Yan Chang, Jia-Jia Zhang, Shao-Bo Xue, Zhong-Wei Lv, Fei Yu, Qing Xia, and Da Fu

SUPPLEMENTAL INFORMATION

Inhibition of USP14 deubiquitinating activity as a potential therapy for tumors with *p53* deficiency

Yu-Shui Ma[1,2*], Xiao-Feng Wang[3*], Yun-Jie Zhang[3], Pei Luo[1], Hui-Deng Long[1], Liu Li[1], Hui-Qiong Yang[1], Ru-Ting Xie[1], Cheng-You Jia[2], Gai-Xia Lu[2], Zheng-Yan Chang[1], Jia-Jia Zhang[2], Shao-Bo Xue[1], Zhong-Wei Lv[2], Fei Yu[2], Qing Xia[3], Da Fu[1#]

Supplemental information contains 3 supplemental figures and legends and online methods.

Supplementary Figure 1

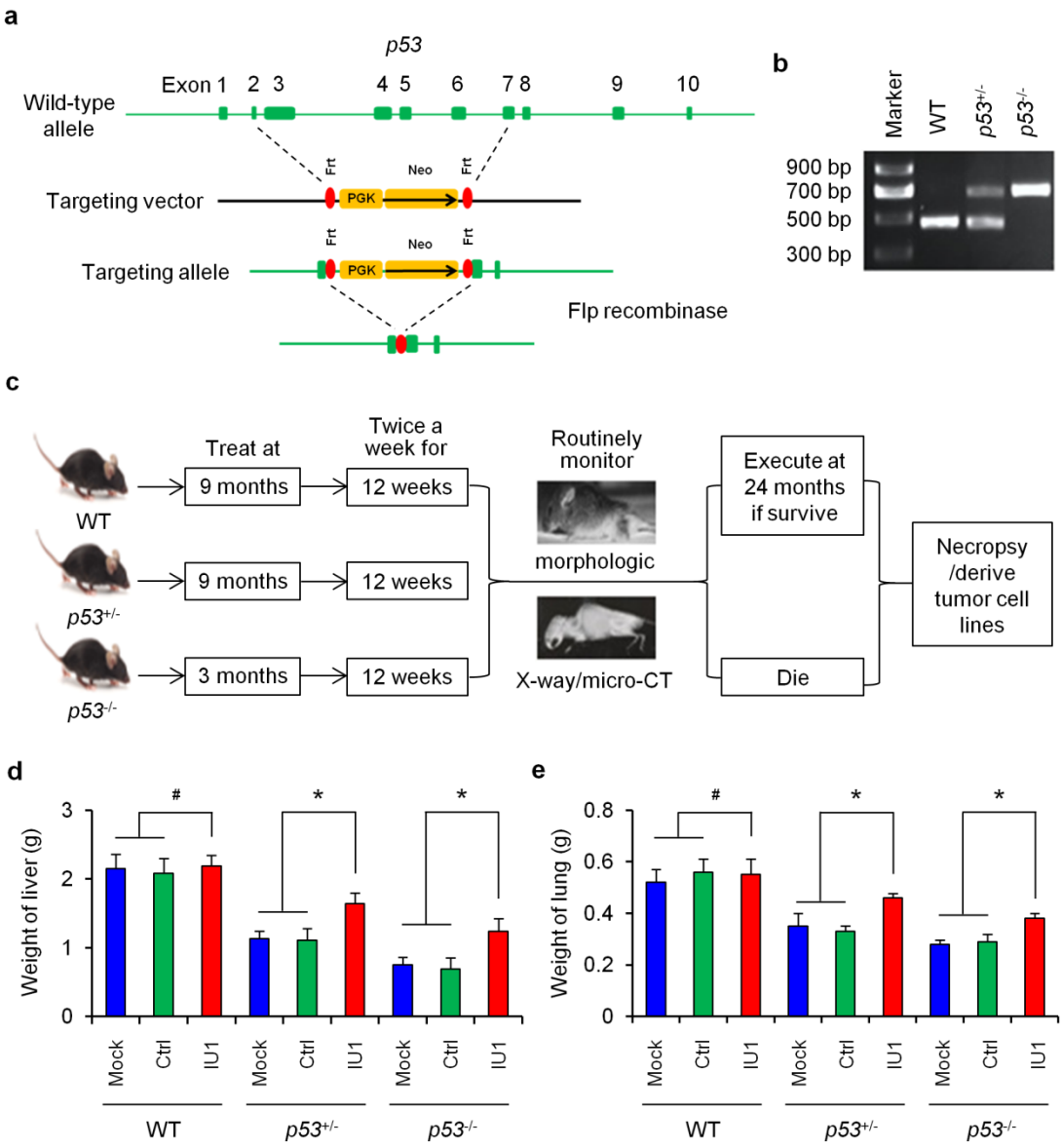

16 **Supplementary Figure 2**

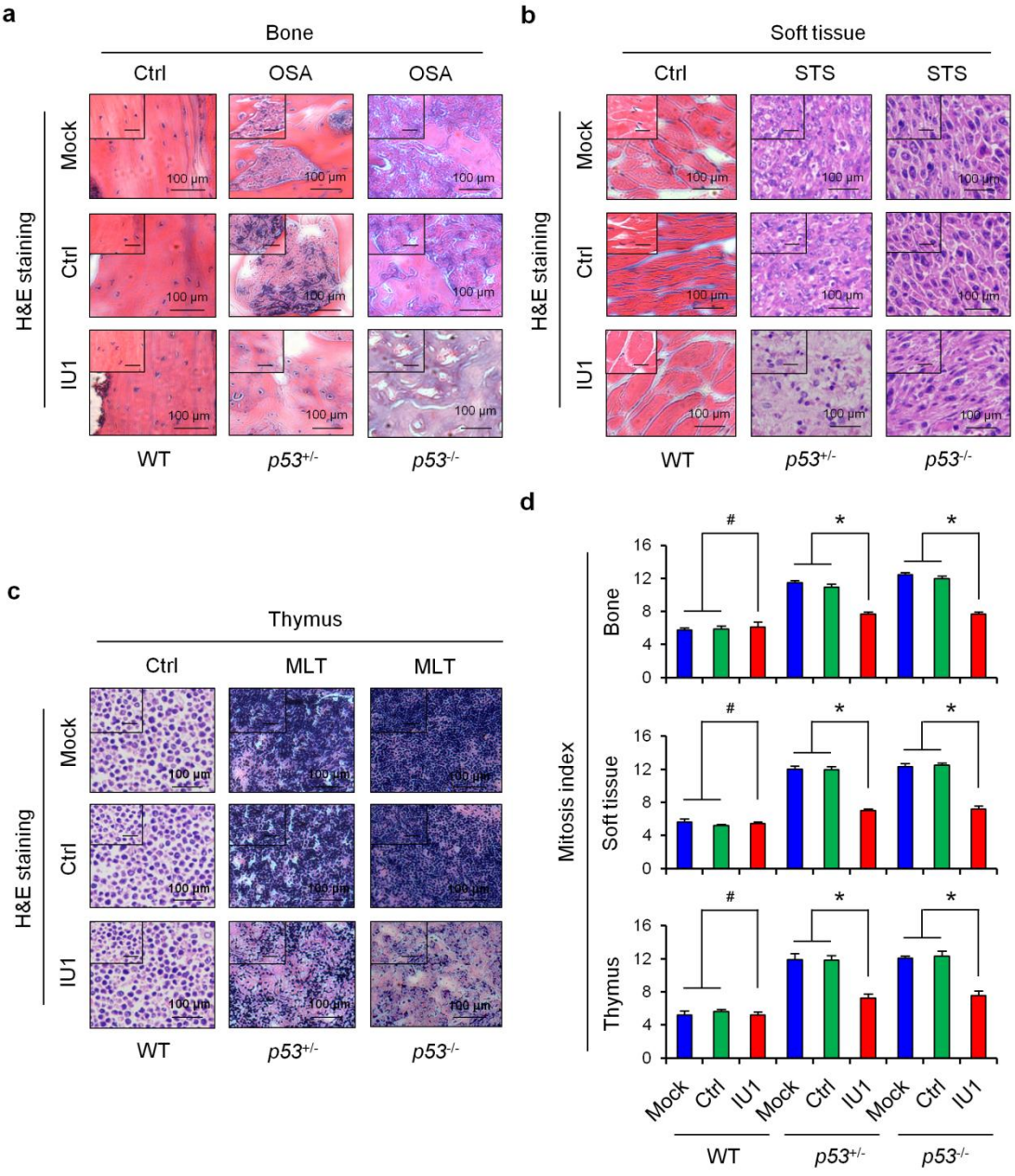

17

18

Supplementary Figure 3

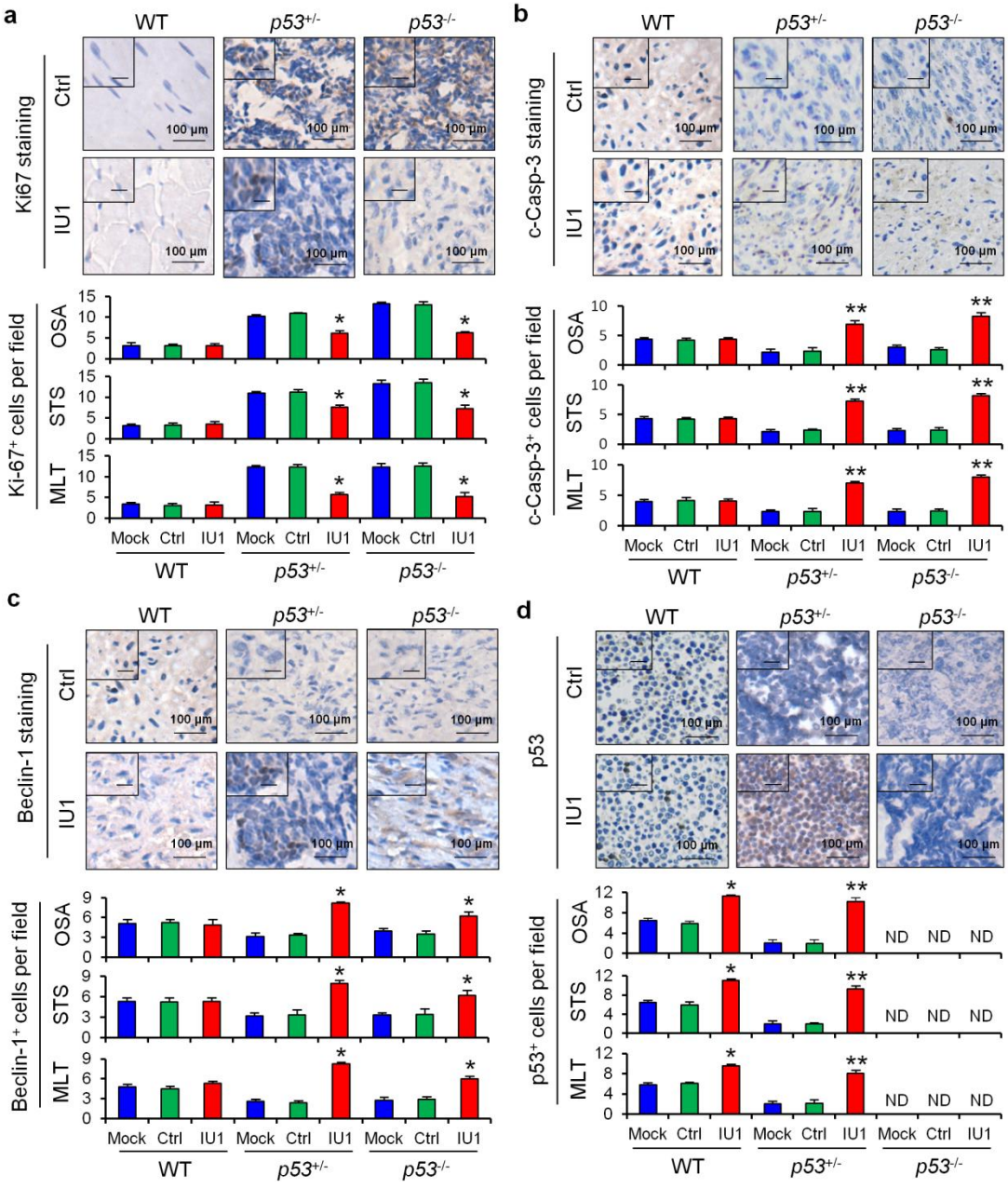

Supplementary legends

Supplementary Figure 1. p53 gene targeting and treatment with IU1 and b-AP15. (a) Scheme for generation of primary tumors with Flp recombinase in FRT-flanked *p53* mice. Homologous recombination between the p53KO-targeting vector and one allele of the endogenous p53 gene results in the replacement of p53 coding sequences between exons 2 and 7 with the neo gene expression cassette and the formation of the $p53^{\Delta}$ mutant allele. (b) Genotypic analysis of offspring from a *p53* heterozygous cross. Tail biopsies were collected at weaning and offspring were screened for the *p53* mutation. (c) Experimental design of generation of primary tumors and treatment with IU1 for tumors with *p53* deficiency. (d, e) Responses to treatment with IU1 as assessed by weight of liver (d) and lung (e). Data shown are the means ± SDs. Statistical analyses were performed with one-way ANOVA (* $P < 0.05$ and $^{\#} P > 0.05$ vs. control).

Supplementary Figure 2. H&E staining and mitosis index analysis in WT or *p53*-deficient mice. (a-c) H&E staining analysis of normal or primary tumors in bone (a), soft tissue (b) and thymus (c) in WT or *p53*-deficient mice with or without treatment with IU1. (d) The mitosis index analysis in WT or *p53*-deficient mice with or without treatment with IU1. Data shown are the means ± SDs. Statistical analyses were performed with one-way ANOVA (** $P < 0.01$ and $^{\#} P > 0.05$ vs. control).

Supplementary Figure 3. IHC staining analysis for p53, Ki67, c-caspase-3 and Beclin-1 in WT or *p53*-deficient mice. IHC staining analysis and quantitative analysis for p53 (a), Ki67 (b), c-caspase-3 (c) and Beclin-1 (d) in WT or *p53*-deficient

mice with or without treatment with IU1 and b-AP15. Data shown are the means ± SDs. Statistical analyses were performed with one-way ANOVA (* $P < 0.05$ and ** $P < 0.01$ vs. control). Ctrl, control; MLT, malignant lymphomas of thymus; Mock, mice without treatment; OSA, osteosarcoma; STS, soft tissue sarcoma; WT, wild type.

ONLINE METHODS

Animal models and genotyping

All experimental procedures were approved by the Institutional Animal Care and Use Committee (IACUC) guidelines at Tongji University School of Medicine (SYDW-19-215).

The *p53*$^{-/-}$ mice in C57BL/6 background, purchased from Jackson Laboratory, were crossed with WT mice and the resulting mice were further intercrossed to generate *p53*$^{+/-}$ mice [1]. Genomic DNA from tail biopsies was genotyped by PCR. The *p53*$^{+/-}$ mice and *p53*$^{-/-}$ mice were used to observe the spontaneous tumor formation, treatment of IU1 and primary cell cultures. IU1 (5mg/kg, 1%DMSO + 30%PEG300 + 1%Tween80 + ddH_2O) was given i.p. twice a week for the number of days indicated. IU1 was purchased from SelleckChem. Mice without any treatment were used as the mock, and mice treated with vehicle (1%DMSO + 30%PEG300 + 1%Tween80 + ddH_2O) were used as the control.

All mice were monitored by X-way, MRI or micro-CT diagnosis for tumor phenotypes weekly up to the age of 24 months before all of the surviving animals were sacrificed. The body and main organs (liver and lung) weight measurements were performed to collect the data when the mouse was died or up to the age of 24 months before all of the surviving animals were sacrificed. Moribund animals or those mice developing obvious tumors before this end point were also sacrificed and necropsied. The tumors were placed in 10% neutral buffered formalin for further histopathological analysis. Tumor histological type was independently confirmed by

two experienced pathologists and tumor volume was calculated using the following formula: volume = length $\times$ width^2 $\times$ 0.52.

All cell mitotic figures within each tumor were counted and are presented as number of mitotic figures per unit area (cm^2). All experimental procedures were approved by the Institutional Animal Care and Use Committee (IACUC) guidelines at Tongji University School of Medicine (SYDW-19-215).

Cell lines

Human osteosarcoma epithelial cell lines U2OS, mouse B lymphoma cell WEH1-231 and human HEK293T cell lines were purchased from the Cell Bank of the Chinese Academy of Sciences (Shanghai, China), and cultured in DMEM media (Invitrogen, Carlsbad, USA) and supplemented with 10 % (v/v) fetal bovine serum (FBS), 100 U/ml penicillin, and 100 mg/ml streptomycin. Cell lines were routinely tested for mycoplasma contamination, and have been authenticated with short-tandem repeat analysis. Derivation of murine thymic lymphoma T-cell lines and primary cultured osteosarcoma cells lines were obtained from *p53*$^{-/-}$ mice and cultured as described previously [2, 3]. Cell culture was conducted at 37 ℃ in a humidified 5% CO_2 incubator.

Cell viability assay

MTS assay (CellTiter 96 Aqueous One Solution reagent) was used to test cell viability as we previously reported [4]. In brief, exponentially growing cells were seeded at 2500 cells/well in a 96-well plate. After incubation for 24 h, U2OS, WEH1-231, PCOC or MTLTC cells were treated with IU1, USP14, shUSP14, COPS5

and/or shCOPS5 plasmids, followed by continuous incubation for 24, 48 or 72 h. MTS reagent (20 μl) was directly added to each well and the incubation was continued for additional 3 h. The absorbance of optical density was measured with a microplate reader (Sunrise, Tecan, Mannedorf, Switzerland) at wavelength 490 nm. Cell viability was calculated by the following formula: cell viability (%) = (average absorbance of treated group − average absorbance of blank) / (average absorbance of untreated group − average absorbance of blank) × 100%.

Flow cytometry (FCM) analysis

Cell apoptosis was determined by flow cytometry analysis [5]. Cells were collected, washed with cold phosphate-buffered saline, fixed in cold 70% ethanol, treated with DNase-free RNase (100 μg/mL, Cat. No. RB473; Sangon Biotech Co., Ltd., Shanghai, China), and stained with 50 μg/mL propidium iodide (Cat. No. P1112; Sangon Biotech) and the Annexin V-APC/7-AAD Kit (Cat. KGA-1025; KeyGEN Biotech, Nanjing, China). The cells were analysed using a Gallios flow cytometer (Beckman Coulter) to quantify the proportion of cells in apoptosis status. To analyze the cell cycle distribution, cells were treated with IU1 for the previously indicated time periods and the harvested cells were fixed with 75% ethanol overnight. Next, the cells were incubated with a 500 μL hypotonic solution containing 50 μg/mL PI, 0.1% sodium citrate, and 0.1% Triton X-100 for 15 min in the dark, and then analyzed by FCM (Becton Dickinson, USA). Data were analyzed using Modfit 2.8 software [6].

Plasmid construction and transfection

Overexpression of USP14, Flag-USP14, COPS5 or HA-COPS5 was performed

using the pMSCV retroviral plasmid. All constructs were confirmed by PCR and Sanger sequencing. The plasmids were transiently transfected into target cells with Lipofectamin 2000 (Life Technologies, Gaithersburg, MD).

To generate stable cell lines with specific gene overexpression or knockdown, the plasmids were packaged into retroviruses with the amphotropic Phoenix packaging cell line and infected into target cells, followed by puromycin/hygromycin selection of infected cells. USP14 or COPS5-knockdown cell lines were generated using short hairpin RNAs and retroviral transduction. Short hairpinRNA (shRNA) a random sequence was set up as a control.

Western blot

Total proteins were extracted from cells following the standard protocol [7]. Protein concentration was measured using the BCA protein assay kit (Thermo Scientific; 23225). The primary antibodies used in this study were as follows: GAPDH (cat. ab8245), USP14 (cat. ab137432), COPS5 (cat. ab210538), p27 (cat. ab32034), DcR2 (cat. ab2019), CDC25C (cat. ab32444), CDC2 (cat. ab18), cleaved caspase-3 (cat. ab2302), pro-caspase-3 (cat. ab13585), BAX (cat. ab32503), BCL-2 (cat. ab32124), Cyclin E1 (cat. ab33911), E2F7 (cat. ab56022), p15 (cat. ab53034), PARP1 (cat. ab32064), HA (cat. ab18181), Cyclin B1 (cat. ab72) and p53 (cat. ab26) from Abcam, AP-1 (cat. 9165), p21 (cat. 2947), p16 (cat. 92803) and Beclin-1 (cat. 3495) from Cell Signaling and Cyclin D1 (cat. 554181) from BD. The goat anti-rabbit IgG (Merck) and goat anti-mouse IgG (Merck) antibodies were used for western blot analyses. Antibody dilutions were 1:1,000 for primary antibodies and 1:5,000 for secondary

antibodies in western blotting. Data are representation of 3-4 independent experiments.

Histology and immunohistochemistry (IHC) analysis

Standard IHC and H&E staining were used to evaluate protein expression levels in tumor samples. Tissues from mice were flushed and fixed in 4% formaldehyde in PBS for 24 h. Samples were then dehydrated and embedded in paraffin, sectioned at 5 μM and processed for H&E staining. The primary antibodies were: Ki-67 (Abcam, ab156956), Beclin-1 (Abcam, ab62557), p53 (Abcam, ab1101), COPS5 (Abcam, ab12323), USP14 (Cell Signaling, 11931), and cleaved-caspase3 (Cell Signaling, 9661). Staining was visualized with ABC Kit Vectastain Elite (Vector) or TSA kit (Invitrogen). Serial sections were stained in parallel with the primary antibody replaced by PBS as controls.

Immunoprecipitation and immunoblotting

For immunoprecipitation assays, cells were pretreated MG132 or IU1 for the previously indicated time periods, and lysed with HEPES lysis buffer (20 mM HEPES, pH 7.2, 50 mM NaCl, 0.5% NP-40, 1 mM NaF and 1 mM dithiothreitol) supplemented with protease-inhibitor cocktail (Roche). Immunoprecipitations were performed using the indicated primary antibody and protein A/G agarose beads (Roche) at 4 ℃. Both lysates and immunoprecipitates were examined using anti-Ub, anti-Flag or anti-HA primary antibodies (Cell Signaling) and the related secondary antibody followed by detection with the chemiluminescence substrate (Millipore). For immunoblotting, total proteins were extracted from cells following the standard

protocol. Cytomembrane free lysate were separated from cells by Native Membrane Protein Extraction Kit (Millipore; 444810). Nuclear and cytoplasmic proteins were separated by Cytoplasmic & Nuclear Extraction Kit (Invent; sc-003) [8]. Protein concentration was measured using the BCA protein assay kit (Thermo Scientific; 23225).

Mass spectrometry

Pellets of U2OS cell expressing Flag-UCH37 from two 150-mm plates were lysed in 50 mM HEPES-KOH (pH8.0), 100 mM KCl, 2 mM EDTA, 0.1% NP-40, 10% glycerol and affinity-purified using Flag-M2 magnetic beads (Sigma-Aldrich). Subsequently, digestion with trypsin (Worthington, Columbus) was performed on-beads. For liquid chromatography-tandem mass spectrometry analysis, peptides were reconstituted in 5% formic acid and loaded onto a 12–15-cm fused silica column with pulled tip packed with C18 reversed-phase material. Peptides were analysed using an LTQ-Orbitrap Velos (Thermo Scientific) or a 6600 Triple TOF (AB SCIEX, Framingham) coupled to an Eksigent NanoLC-Ultra HPLC system and a nano-electrospray ion source (Proxeon Biosystems, Thermo Fisher Scientific). Peptides were eluted from the column using a 90–100-min gradient of acetonitrile in 0.1% formic acid. The lyophilized peptide mixture was re-suspended in water with 0.1% formic acid (v/v) and its content was estimated by UV light spectral density at 280 nm, then 3 μg of the digest peptides were analyzed by nano-liquid chromatography-tandem mass spectrometry (LC-MS/MS) on LTQ Orbitrap Velos Pro mass spectrometer [9-11]. Raw data was processed by Maxquant software (1.3) and

then used for database and spectral library searching using Andromeda peptide search engines. The Maxquant peptide and protein quantification results files were imported into Perseus software (version 1.5.1.6) for further analysis [12].

RNA extraction and quantitative PCR (qPCR)

RNA was extracted using TRIzol (ThermoFisher Scientific) following the manufacture's protocol, and then subjected to cDNA synthesis using iScript kit (Bio-rad). RNA concentration was measured using a NanoDrop2000 spectrophotometer (Thermo Fisher Scientific, Waltham, MA, USA). Electrophoresis on 1.5% denaturing agarose gels was performed to evaluate the quality of all RNA specimens. The cDNA was obtained from total RNA by reverse transcription, and the final RNA concentration used in the quantitative PCR reaction was 10 ng, Real-time PCR was performed using the iTag universal SYBR Green kit (Bio-rad) and subsequently analyzed in a CFX Connect system (Bio-rad). Sequences of PCR primers are as following: GAPDH: Forward, 5'-ACCCAGAAGACTGTGGATGG-3', Reverse, 5'-TTCTAGACGGCAGGTCAGGT-3'; USP14: Forward, 5'-GGCGTGTGGAGATGTATAAC-3, Reverse, 5'-CAGCTCAGCACTATCCAGAC-3' and COPS5, Forward, 5'-GTCATGTGGTTGCTGTGATG-3', Reverse, 5'-AGGTGACGTGACTGAATGAG-3'. GAPDH were used as the endogenous controls, and the $2^{-\Delta\Delta CT}$ method was used to analyze expression levels [13].

Imaging

In the animal studies, we used the dual tube/detector micro-CT system that has

been described in detail elsewhere [14]. The x-ray parameters were 80 kVp, 160 mA, and 10ms per exposure, and the radiation dose associated with the micro-CT scan was 16 cGy. MRI experiments were performed on a Bruker BioSpec 7.0 Tesla 30 cm clear bore USR (Ultra Shielded Refrigerated) horizontal bore Superconducting Magnet System [15]. The Bruker-made 23-mm ID birdcage volume radiofrequency coil was used for both radiofrequency excitation and receiving. Animals were anesthetized throughout the imaging procedure through the inhalation of a mixture of 1.5% isoflurane into medically supplied air.

Statistical analysis

Measurement data was expressed as mean ± S.D. (standard deviation). Categorical data were reported as numbers and percentages. Analysis of two samples was performed with unpaired two-tailed Student t test for equal variance, or t test with Welch's correction for heterogeneity of variance. The chi-square test was used to evaluate the difference among different groups. Univariate survival analysis of overall survival was carried out using the Kaplan-Meier method. Spearman's correlation coefficient was used to test the relationship of two independent groups. All calculations were performed with the Prism 6.0 GraphPad or SPSS 20.0 software program (SPSS Inc, Chicago, IL, USA). The level of significance was set as $P < 0.05$.

Supplementary References

[1] Jacks T, Remington L, Williams BO, Schmitt EM, Halachmi S, Bronson RT, *et al*. Tumor spectrum analysis in p53-mutant mice. Curr Biol. 1994, 4(1): 1-7.

[2] Jinadasa R, Balmus G, Gerwitz L, Roden J, Weiss R, Duhamel G. Derivation of thymic lymphoma T-cell lines from $Atm^{-/-}$ and $p53^{-/-}$ mice. J Vis Exp. 2011, (50): 2598.

[3] Ma O, Cai WW, Zender L, Dayaram T, Shen J, Herron AJ, *et al*. MMP13, Birc2 (cIAP1), and Birc3 (cIAP2), amplified on chromosome 9, collaborate with p53 deficiency in mouse osteosarcoma progression. Cancer Res. 2009, 69(6): 2559-67.

[4] Liao Y, Liu N, Hua X, Cai J, Xia X, Wang X, *et al*. Proteasome-associated deubiquitinase ubiquitin-specific protease 14 regulates prostate cancer proliferation by deubiquitinating and stabilizing androgen receptor. Cell Death Dis. 2017, 8(2): e2585.

[5] Ma YS, Yu F, Zhong XM, Lu GX, Cong XL, Xue SB, *et al*. miR-30 Family Reduction Maintains Self-Renewal and Promotes Tumorigenesis in NSCLC-Initiating Cells by Targeting Oncogene TM4SF1. Mol Ther. 2018, S1525-0016(18): 30447-7.

[6] Ma YS, Huang T, Zhong XM, Zhang HW, Cong XL, Xu H, *et al*. Proteogenomic characterization and comprehensive integrative genomic analysis of human colorectal cancer liver metastasis. Mol Cancer. 2018, 17(1): 139.

[7] Ma YS, Lv ZW, Yu F, Chang ZY, Cong XL, Zhong XM, *et al*. MiRNA-302a/d

inhibits the self-renewal capability and cell cycle entry of liver cancer stem cells by targeting the E2F7/AKT axis. J Exp Clin Cancer Res. 2018, 37(1): 252.

[8] Choi YS, Hoon Jeong J, Min HK, Jung HJ, Hwang D, Lee SW, *et al*. Shot-gun proteomic analysis of mitochondrial D-loop DNA binding proteins: identification of mitochondrial histones. Mol Biosyst. 2011, 7(5): 1523-36.

[9] Yu Z, Liu N, Wang Y, Li X, Wang X. Identification of neuroglobin-interacting proteins using yeast two-hybrid screening. Neuroscience. 2012, 200: 99-105.

[10] Tian XP, Jin XH, Li M, Huang WJ, Xie D, Zhang JX. The depletion of PinX1 involved in the tumorigenesis of non-small cell lung cancer promotes cell proliferation via p15/cyclin D1 pathway. Mol Cancer. 2017, 16(1): 74.

[11] Luo P, Lu G, Fan LL, Zhong X, Yang H, Xie R, *et al*. Dysregulation of TMPRSS3 and TNFRSF11B correlates with tumorigenesis and poor prognosis in patients with breast cancer. Oncol Rep. 2017, 37(4): 2057-2062.

[12] Sun X, Zhang H, Luo L, Zhong K, Ma Y, Fan L, *et al*. Comparative proteomic profiling identifies potential prognostic factors for human clear cell renal cell carcinoma. Oncol Rep. 2016, 36(6): 3131-3138.

[13] Livak KJ, Schmittgen TD. Analysis of relative gene expression data using real-time quantitative PCR and the $2^{-\Delta\Delta Ct}$ method. Methods, 2001. 25(4): 402–408.

[14] Badea CT, Johnston S, Johnson B, Lin M, Hedlund LW, Johnson GA. A dual micro-CT system for small animal imaging. Proc SPIE. 2018, 6913: 691342.

[15] Ni J, Ramkissoon SH, Xie S, Goel S, Stover DG, Guo H, *et al*. Combination

inhibition of PI3K and mTORC1 yields durable remissions in orthotopic patient-derived xenografts of HER2-positive breast cancer brain metastases. Nat Med. 2016, 22(7): 723–726.